26. D. V. Nalivkin, *The Geology of the USSR* (Pergamon, New York, 1960).
27. W. W. Patton, Jr., and J. M. Hoare, *U.S. Geol. Surv. Prof. Pap. 600-D* (1968), p. D147.
28. C. H. Nelson, personal communication.
29. R. D. Muench, R. L. Charnell, J. D. Cline, L. Coachman, *J. Geophys. Res.*, in press.
30. R. E. Laplante, *Am. Assoc. Pet. Geol. Bull. 58* (1974), p. 1281.
31. B. Tissot, B. Durand, J. Espitalie, A. Combaz, *ibid.*, p. 499.
32. J. M. Hunt, *Pet. Eng. Int.* (March 1975), p. 112.
33. B. J. Moore, R. D. Miller, R. D. Shrewsbury, *U.S. Bur. Mines Inf. Circ. 8302* (1966), p. 1.
34. D. R. Schink, N. L. Guinasso, Jr., J. J. Sigalove, N. E. Cima, paper presented at the third Offshore Technology Conference of the American Institute of Mining, Metallurgical, and Petroleum Engineers, 1971.
35. R. W. Macdonald and C. S. Wong, *Chemistry and Physics of Aqueous Gas Solutions*, W. A. Adams, Ed. (Electrochemical Society, Princeton, N.J., 1975), p. 214.
36. The fractional mass loss (Δm) out of a bubble per unit time (Δt) is given by

$$\Delta m = \frac{A P_t \alpha M D}{R T \Delta h} \Delta t$$

where A is the bubble surface area, P_t is the total gas pressure in the bubble (hydrostatic + surface tension), α is the Bunsen coefficient, M is the molecular weight of the component, D is the molecular diffusivity of the component in water, R is the gas constant, T is the absolute temperature, and Δh is the boundary film thickness. Since $\Delta m/M$ is equal to the concentration increase (ΔC_i) per unit time, the concentration ratio of two components is simply proportional to the respective partial pressures, solubilities (Bunsen coefficients), and molecular diffusivities as shown in Eq. 1.
37. P. A. Witherspoon and L. Bonoli, *Ind. Eng. Chem.* **8**, 589 (1969).
38. *Oil Gas J.* **69**, 57 (May 1971).
39. V. F. Nikonov, *Dokl. Akad. Nauk SSSR* **206**, 234 (1972).

40. This study was supported by the Bureau of Land Management through interagency agreement with the National Oceanic and Atmospheric Administration, under which a multiyear program responding to needs of petroleum development of the Alaskan continental shelf is managed by the Outer Continental Shelf Environmental Assessment Program (OCSEAP) Office. We wish to express our gratitude to T. H. McCulloh, K. Kvendvolden, M. Marlow, and G. Claypool of the Geological Survey for their critical review and helpful suggestions in the preparation of this manuscript. We are also indebted to Captain C. Upham and the officers of the NOAA research vessel *Discoverer* for their diligence and support during the detailed investigations of the seep, and to C. Katz and M. Pizzello for sample analyses and data reduction.

24 May 1977; revised 22 August 1977

Water Vapor Maser "Turn-On" in the HII Region W3 (OH)

Abstract. *A line in the water vapor maser spectrum of the HII region W3 (OH) was observed to increase in brightness over an 8-day period and then decline to its original intensity over the following 4 weeks. The intensity variation can be explained by a simple maser model, with an impulse of energy suddenly applied. The observed time scale and energy output are consistent with a maser on the outskirts of a dust cocoon surrounding an O5 star, with a momentary "leak," lasting a day or two, supplying the necessary energy.*

Naturally occurring masers in interstellar clouds have been demonstrated for a number of different molecular transitions, the 18-cm OH lines and the 1.35-cm H_2O rotational line being the most intense examples (*1*). The masers are commonly found in ionized hydrogen (HII) regions where star formation is still in process, but are also found in association with late-type red giant stars. Both the OH and H_2O masers, when found in HII regions, have intense infrared sources (presumably protostars) in their proximity.

There is strong reason to believe that the masering phenomenon is short-lived and occurs early in the life cycle of a star. The H_2O masers in particular require high local gas densities ($\sim 10^{10}$ molecules of H_2 per cubic centimeter) in order to populate the rotational levels which lie roughly 450 cm^{-1} above the ground state. The total power output from the OH and H_2O masers in the radio line is an appreciable fraction of 1 solar luminosity ($\sim 10^{-4}$ to 1 $L_\odot$) and a copious source of pump energy is required. Typically, the masers consist of a cluster of individual "hot spots," each having an apparent size of approximately 1 astronomical unit (1 A.U. = 1.5×10^{13} cm) with the group spread over a total dimension of approximately 10^3 to 10^4 A.U. The group thus has a total dimension characteristic of the solar system. The pump mechanism has not been demonstrated, although infrared radiation and collisional pumping have both been proposed. The apparent size of each hot spot may not necessarily represent the true maser source size, and several authors (*2*) have shown that for simple, uniform models of H_2O masers, the true size of the masering region could be of the order of 50 times the apparent size. The H_2O masers, in particular, are observed to vary rapidly with time (*3*), and we report here the first complete "turn-on" sequence observed for an individual maser spot.

During the course of an observing run with the 120-foot (37-m) radio telescope of the Haystack Observatory in Westford, Massachusetts, the increasing intensity of a line in the H_2O spectrum of the HII region W3 (OH) (associated with the larger HII complex IC1795) was noted and was monitored closely for a 10-day period. The Haystack telescope then became less available, but the 26-m telescope of the Naval Research Laboratory (NRL) at Maryland Point was used at frequent intervals for the next 4 weeks, allowing a complete set of observations to be brought together.

The Haystack antenna was equipped with a left circularly polarized Cassegrain feed and a traveling wave maser preamplifier having a system temperature in the range 100° to 200°K. The sensitivity of the antenna at a wavelength of 1.35 cm is 14 jansky of total flux density per degree Kelvin of antenna temperature (1 jy = 10^{-26} watt m^{-2} $hertz^{-1}$). The spectrometer comprised a 1024-channel autocorrelator which with Hanning weighting of the autocorrelation function provided a velocity resolution

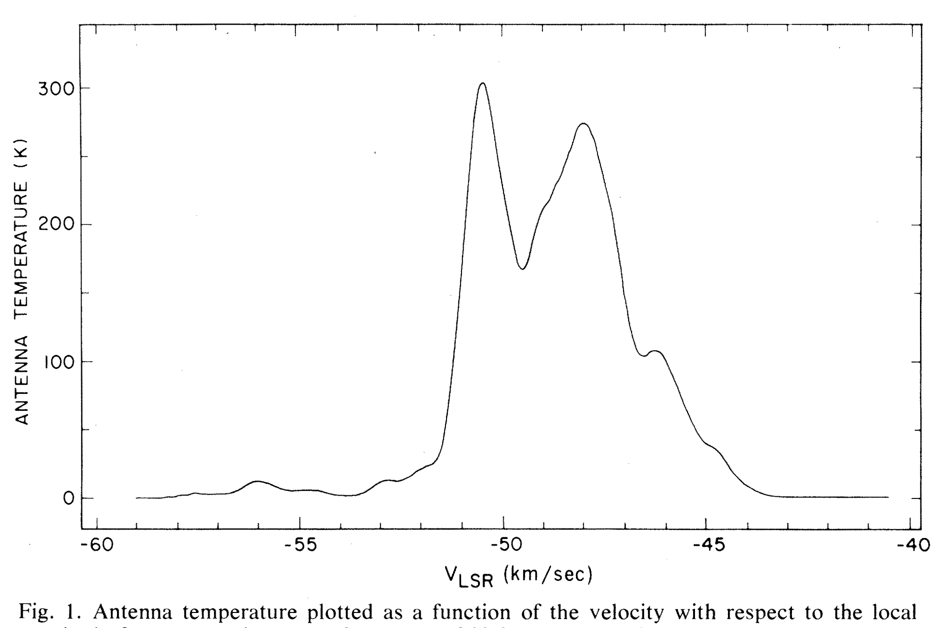

Fig. 1. Antenna temperature plotted as a function of the velocity with respect to the local standard of rest, assuming a rest frequency of 22,235.080 Mhz, for the source W3 (OH). The spectrum was taken on 13 May 1977 and represents a total of 3 minutes of integration time and an effective velocity resolution of 0.066 km/sec. The strongest line is the −50.4 km/sec feature; the next strongest is the −48 km/sec feature, on whose shoulder the −46 km/sec feature is visible.

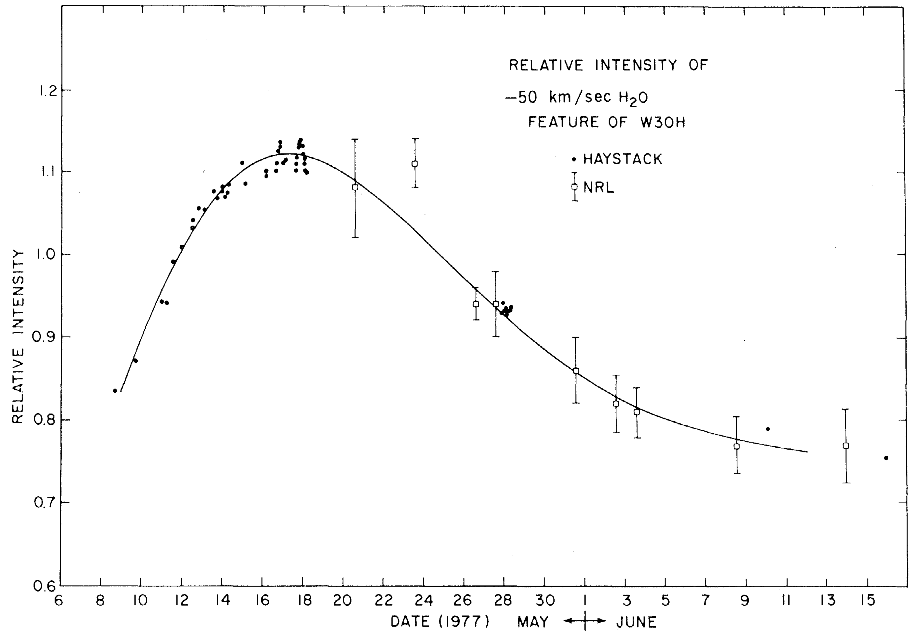

Fig. 2. Ratio of the peak antenna temperature of the −50.4 km/sec feature in the H_2O spectrum of W3 (OH) with respect to that of the −48 km/sec feature plotted as a function of time from 8 May to 16 June 1977. The Haystack data have been corrected to a resolution of 0.066 km/sec when a 6-Mhz bandwidth was used. No resolution correction was applied to the NRL data.

of 0.07 km/sec for a 2-Mhz bandwidth. The receiver was operated in the total power mode, taking the difference between on-source and off-source spectra. The duration of individual observations ranged between 3 and 5 minutes throughout the observing period.

The 26-m NRL antenna, with a sensitivity of 12 jy per degree Kelvin, utilized a beam-switched mixer radiometer, having a single side-band system temperature of 2200°K. The feed was a linearly polarized horn, and the receiver could be rotated about the reflector axis to analyze the linear polarization of the received wave. Spectral analysis was provided by a bank of 192 contiguous adjacent 15-khz channels providing a velocity resolution of 0.2 km/sec. The observing procedure was similar to that used at the Haystack station.

A water vapor spectrum of W3 (OH) taken at the Haystack Observatory on 13 May 1977 is shown in Fig. 1. The antenna temperature is plotted as a function of the velocity of the source with respect to the local standard of rest in kilometers per second. The spectrum shown comprises a number of confused and overlapping features in the velocity range −58 to −44 km/sec. The asymmetry of the feature at −48 km/sec indicates the presence of more than one maser component in the line, while the relative symmetry of the line at −50.4 km/sec would tend to indicate that a good proportion of the power radiated at that velocity comes from a single maser spot.

The amplitude of the feature at −50.4 km/sec was found to increase rapidly with respect to that of the −48 km/sec feature over the period of 4 to 5 days following 8 May 1977. It reached a maximum on approximately 17 May and then diminished over the following 4 weeks. The data from both observatories are summarized in Fig. 2, which shows the ratio of the peak antenna temperature of the −50.4 km/sec feature with respect to that of the −48 km/sec feature as a function of time from 8 May to 16 June 1977. The experimental uncertainties of the Haystack data ranged from 0.3 to 0.5 percent, depending on the integration time, but are not shown because of the large number of individual points. The NRL measurements are daily averages, with each point representing several hours of data, and necessarily have larger uncertainties because of the higher system temperature.

Taking line ratios avoids calibration difficulties caused by variable atmospheric attenuation and instrumental gain. Furthermore, since it is known that all the features are confined within 2 arc-seconds (*4*), an angular separation that is small compared to the antenna beamwidths, pointing errors are also negligible. Nevertheless, all maser lines are subject to time variations, and it is necessary to establish which line has relatively constant intensity over the duration of the observations. The −48 km/sec line appears to meet this criterion, since it retained the same asymmetric line shape and absolute measurements of its intensity throughout the observing period gave peak values that were constant to within experimental uncertainties. The −46 km/sec line was definitely not constant in intensity but diminished slowly throughout the observing period. In the data of Fig. 2 there seem to be short time variations in the ratio of the two features outside the statistics. The variations appear to be real, but verification studies are in progress.

Linear polarization was measured at NRL by rotating the feed. The −48 km/sec feature exhibited 10 ± 5 percent linear polarization at position angle −10° ± 35°, a value consistent with the more precise measurements of Bologna *et al.* (*5*). The polarization of the −50.4 km/sec feature relative to the −48 km/sec one could be determined with greater accuracy. The polarization of the −50.4 km/sec feature appeared to diminish steadily over the observing period, from 20 percent on 20 May to 6 percent on 14 June, with no changes in position angle. The high degree of correlation between flare intensity and polarization is similar to that reported by Bologna *et al.* for the 2 km/sec feature of W75S. The polarization variation thus confirms the reality of the flux variation.

Models for H_2O masers must meet severe energy requirements. The observed luminosity (L) for line radiation from the W3 (OH) complex is $10^{-3} L_{\odot}$, and there are cases such as W49 in which the total line luminosity is approximately 1 $L_{\odot}$ (*4*). A completely efficient pump mechanism is unlikely, and so a copious energy source is needed. A newly formed O5 star ($L \approx 8 \times 10^5 L_{\odot}$) would provide the necessary energy source, since such a star in its early stages would probably be surrounded by a dust cocoon that would convert the star's radiation from visible and ultraviolet wavelengths into the infrared region of the spectrum. Such condensations have apparently been observed (*6*), frequently in close association with H_2O masers. If such a star is still accreting matter, the maser complex might well be on the periphery, receiving thermal energy that serves as the pump.

Various pump mechanisms have been proposed, including pumping by infrared radiation, supplied either externally or internally (*7*), and collisional pumping (*8*). The cocoon may be subject to Rayleigh-Taylor instabilities, and we have investigated a very simple model that derives its pump energy from a brief heat pulse that could come from a momentary break in the cocoon. We assume that (i) the heat pulse is effectively a delta function in time and space applied to a masering cloud of uniform density,

(ii) the energy diffuses according to the diffusion equation with no time variation of the thermal diffusion constant, (iii) the pump mechanism is collisional and varies directly as molecular velocity and thus as the square root of temperature, and (iv) the maser is saturated—that is, the principal relaxation from the upper masering level is through induced maser transitions. The result of the calculation is given by the solid curve in Fig. 2, which fits the data very well throughout the observing sequence. Only the time scale (that is, the thermal diffusion constant) is varied in the model; otherwise there are no free parameters. Other models have been tried, including a heat pulse of length comparable to the diffusion time and a heat pulse with radiational pumping. None of these models give as satisfactory a fit to the data.

The quantitative requirements of the model seem reasonable. If one postulates an O5 star with $L = 8 \times 10^5 L_{\odot}$ and an ionized cavity 100 A.U. in radius, and the break in the cocoon grows for 1 day at a velocity of 1 km/sec and then heals at the same rate, the heat pulse would be sufficiently short. The supply of energy would be equal to the observed luminosity change (assuming an isotropic maser). It is interesting to note that the maser would be the principal exit channel for the energy in the heat pulse, since the shorter-wavelength radiation propagates too slowly to escape until the temperature drops below 200°K. The characteristic time of the observed variation is consistent with such a model, since the maser dimension is 10^{13} to 10^{15} cm, depending on the ratio of observed size to true size. A shock wave with a velocity of 10 km/sec would require months to years to traverse the region, while radiation traveling unimpeded would require 10^3 to 10^5 seconds, which is too fast. Thus, diffusion of radiation is more consistent with the observed time scale. The cocoon model for W3 (OH) itself does have difficulties, as Forster *et al.* (*9*) have pointed out. Not enough infrared radiation seems to be coming from the proposed cocoon star. The calculated curve shown in Fig. 2 does not depend on the cocoon star model, of course, since any pulsed source of energy would serve.

A. D. HASCHICK, B. F. BURKE
Research Laboratory of Electronics, Department of Physics, Massachusetts Institute of Technology, Cambridge 02139

J. H. SPENCER
E. O. Hulburt Center for Space Research, Naval Research Laboratory, Washington, D.C. 20375

References and Notes

1. J. M. Moran, B. F. Burke, A. H. Barrett, A. E. E. Rogers, J. A. Ball, J. C. Carter, D. D. Cudaback, *Astrophys. J. Lett.* **152**, L97 (1968); B. F. Burke, D. C. Papa, G. D. Papadopoulos, P. R. Schwartz, S. H. Knowles, W. T. Sullivan, M. L. Meeks, J. M. Moran, *ibid.* **160**, L63 (1970). See also reviews by B. F. Burke [*Int. Astron. Union Symp. 60* (1975), p. 252] and J. M. Moran [in *Frontiers of Astrophysics*, E. Avrett, Ed. (Harvard Univ. Press, Cambridge, 1976), p. 385].
2. P. Goldreich and D. A. Keely, *Astrophys. J.* **174**, 517 (1972); M. M. Litvak, *ibid.* **182**, 711 (1973).
3. D. Buhl, L. E. Snyder, P. R. Schwartz, A. H. Barrett, *Astrophys. J. Lett.* **158**, L97 (1969); W. T. Sullivan III, *ibid.* **166**, 321 (1971); R. H. Gammon, *Astron. Astrophys.* **50**, 71 (1976).
4. J. M. Moran *et al.*, *Astrophys. J.* **185**, 535 (1973).
5. J. M. Bologna, K. J. Johnston, S. H. Knowles, S. A. Mango, R. M. Sloanaker, *ibid.* **199**, 86 (1975).
6. C. G. Wynn-Williams and E. E. Becklin, *Publ. Astron. Soc. Pac.* **86**, 5 (1974); R. L. Brown and B. Zuckermann, *Astrophys. J. Lett.* **202**, L125 (1975).
7. M. M. Litvak, *Science* **165**, 855 (1969); P. Goldreich and J. Kwan, *Astrophys. J.* **191**, 93 (1974).
8. T. de Jong, *Astron. Astrophys.* **26**, 297 (1973).
9. J. R. Forster, W. J. Welch, M. C. H. Wright, *Astrophys. J. Lett.* **215**, L121 (1977).
10. We thank all those who sacrificed observing time or helped obtain spectra in order to fill up gaps in the data. These include W. Dent, P. Ho, K. J. Johnston, S. E. Kleinmann, T. Balonek, N. Cohen, J. Garcia-Barreto, P. Greenfield, M. Schneps, P. Solomon, J. M. Bologna, C. H. Mayer, and N. J. Santini. Special thanks are due to T. Giuffrida, who contributed a major block of observing time and supervised many observations at the Haystack Observatory. Thanks are also due to the Haystack staff and operators who assisted in the observations and helped obtain extra observing time. This research was supported by a grant from the National Science Foundation. The Haystack Observatory of the Northeast Observatory Corporation is supported by the National Science Foundation.

9 August 1977; revised 12 September 1977

Hominoid Enamel Prism Patterns

Abstract. *Analysis of enamel prism patterns in a selected series of extant hominoids reveals that pongids have a pattern distinctively different from that of* Homo sapiens. *The pattern for a Miocene hominoid,* Ramapithecus, *is very similar to that seen in* Homo sapiens. *The finding allows a new approach to the evaluation of isolated teeth.*

Teeth are often the most abundant, and frequently the only, remains of fossil primates found; thus it is essential that every piece of information from these particularly indestructible structures be evaluated. At present, most of our knowledge of Miocene hominoids, including possible ancestors of later hominids, is based on dental remains. Correct interpretation of these remains is crucial to understanding hominid phylogeny, and this is especially true when isolated remains are analyzed. Data obtained from these specimens have often led to a variety of conflicting interpretations. Morphological analysis of occlusal surfaces, especially when isolated teeth are evaluated, may not provide definitive answers regarding either adaptation or phylogeny. For a more adequate appraisal additional analytic methods and techniques must be used. Scanning electron microscopy of enamel prism patterns is one such technique.

The study of enamel prism patterns is not new. Tomes (*1*) was the first to attempt an analysis of the structure of enamel as a possible taxonomic character in the marsupials. Later, Carter (*2*) applied Tomes's techniques to the study of a series of primates, including a number of fossil prosimians. The data obtained from the study by Carter led Regan (*3*) to devise a new classification of the order Primates. However, these studies were not well received by other researchers and had little, if any, effect on classification or theories of primate evolution. The reason for this was, perhaps, a lack of understanding of the ultrastructure of enamel in man and other mammals.

It was not until the advent of the scanning electron microscope (SEM) that researchers could begin to understand the development and ultrastructural features of enamel, especially the enamel prism. The work of Boyde (*4*) has done much to provide a more comprehensive understanding of enamel structure in mammals. Analyses with the SEM of developing and mature enamel have documented the fact that specific enamel prism patterns do exist and can be used as a taxonomic indicator (*4*). The purpose of the research reported here was to develop a nondestructive method of analysis to evaluate the enamel of primates, with emphasis on studying isolated teeth. The work of Carter (*2*), Shobusawa (*5*), and Boyde (*4, 6*) provided data which indicated that a study of the enamel prism patterns could yield reproducible results. Therefore, a study was conducted to determine the enamel prism patterns in a select sample of primate teeth, with emphasis on Hominoidea.

Molar and premolar teeth were obtained from a number of extant and extinct primates. These specimens were cleaned in absolute alcohol and acetone for 1 hour each and were then etched in a 10 percent solution of hydrochloric acid for 2.5 minutes. This procedure usually removed the outer, prismless layer. The specimens were subsequently washed in